Phys Chem Minerals (2006) 32: 710–720
DOI 10.1007/s00269-005-0046-x

ORIGINAL PAPER

Émilie Gaudry · Philippe Sainctavit · Farid Juillot
Federica Bondioli · Philippe Ohresser · Isabelle Letard

From the green color of eskolaite to the red color of ruby: an X-ray absorption spectroscopy study

Received: 27 January 2005 / Accepted: 16 October 2005 / Published online: 10 December 2005

Abstract The best known cause for colors in insulating minerals is due to transition metal ions as impurities. As an example, Cr^{3+} is responsible for the red color of ruby (α-Al_2O_3:Cr^{3+}) and the green color of eskolaite (α-Cr_2O_3). Using X-ray absorption measurements, we connect the colors of the $Cr_xAl_{2-x}O_3$ series with the structural and electronic local environment around Cr. UV–VIS electronic parameters, such as the crystal field and the Racah parameter B, are related to those deduced from the analysis of the isotropic and XMCD spectra at the Cr $L_{2,3}$-edges in $Cr_{0.07}Al_{1.93}O_3$ and eskolaite. The Cr–O bond lengths are extracted by EXAFS at the Cr K-edge in the whole $Cr_xAl_{2-x}O_3$ ($0.07 \leq x < 2$) solid solution series. The variation of the mean Cr–O distance between $Cr_{0.07}Al_{1.93}O_3$ and α-Cr_2O_3 is evaluated to be 0.01_5 Å (≈1%). The variation of the crystal field in the $Cr_xAl_{2-x}O_3$ series is discussed in relation with the variation of the averaged Cr–O distances.

Keywords XAFS · Ruby · Color of minerals

Introduction

The color of minerals is due to the interaction of light with matter. When light goes through ruby (α-Al_2O_3:Cr^{3+}), the whole yellow-green and violet radiations are absorbed, while red and few blue radiations are transmitted. Therefore, ruby is red with a slight purple overtone. On the contrary, red light is absorbed in eskolaite (α-Cr_2O_3), so that this mineral looks green. Although it is now well known that color in ruby and eskolaite is due to the chromium ions (Nassau 1983; Burns 1993), a question remains unexplained. Why does the same chromium chromophore ion, with the same valence state and the same kind of distorted octahedral site, yield a red color in ruby and a green one in eskolaite?

In such oxide minerals, color is generally interpreted within the ligand field theory. This model is based on an electrostatic interaction between the central cation and the ligands of its coordination sphere. It is based mainly on the geometry and the symmetry around the central cation. This theory has been applied successfully to predict the number of 3d–3d transitions in optical absorption spectra and to identify the corresponding absorption bands (Lever 1984). Moreover, this theory enables an empirical calculation of the transition energies (Liehr 1963). The UV–VIS absorption spectra of Cr^{3+}-containing materials present two main absorption bands, which are already well explained by the ligand field theory applied to the system Al_2O_3:Cr^{3+} (Poole 1964; Poole and Itzel 1963; McClure 1962, 1963; Reinen 1969; Sugano and Peter 1961; Liehr 1963; MacFarlane 1963; Graham 1960). The spectroscopic term of the fundamental state for the free Cr^{3+} coloring ion in spherical symmetry is ^4F. In the octahedral symmetry, ^4F is split into three states of increasing energies that are $^4A_{2g}$, $^4T_{2g}$ and $^4T_{1g}$. The symmetry of the ground state is $^4A_{2g}$. The absorption band at lower energy, labeled ε_1, arises from $^4A_{2g}$ toward $^4T_{2g}$ transitions. The broad band at higher energy, labeled ε_2, arises from $^4A_{2g}$ toward $^4T_{1g}$ transitions. The crystal field parameter Δ and the Racah parameter B are extracted from the values of ε_1 and ε_2 within the framework of the crystal field model. The Δ parameter is given by the energy ε_1. The B parameter is given by $B = [(\epsilon_2 - \epsilon_1)/3][(2\epsilon_1 - \epsilon_2)/(9\epsilon_1 - 5\epsilon_2)]$ (Marfunin 1979; Reinen 1969). The optical data given by Reinen (1969) lead to $\Delta = 2.24$ eV

É. Gaudry · P. Sainctavit (✉) · F. Juillot · I. Letard
Laboratoire de Minénalogie-Cristallographie,
Université Pierre et Marie Curie, UMR 7590,
4 place Jussieu, 75252 Paris Cedex 05, France
E-mail: philippe.sainctavit@lmcp.jussieu.fr

P. Sainctavit · P. Ohresser
LURE, Bât 209D Centre Universitaire,
B.P. 34, 91898 Orsay Cedex, France

F. Bondioli
Dipartimento di Ingegneria dei Materiali e dell'Ambiente,
Universitá di Modena e Reggio Emilia,
Via Vignolese 905, 41100 Modena, Italy

(18,070 cm^{-1}) for ruby and $\Delta = 2.07$ eV (16,700 cm^{-1}) for α-Cr_2O_3, while the Racah parameter B is $B = 0.080$ eV (645 cm^{-1}) for ruby and $B = 0.058$ eV (468 cm^{-1}) for α-Cr_2O_3. The ratio Δ/B increases when the concentration x of chromium in $Cr_xAl_{2-x}O_3$ increases.

Despite the success of the ligand field theory, some points remained misunderstood. Liehr (1963) tried to sort the minerals by increasing values of the crystal field Δ and the Racah parameter B given by optical spectroscopy. He wanted to make an analogy with the spectroscopic and the nephelauxetic series in solutions but found irregular changes for the crystal field Δ and for the Racah parameter B in his crystalline series. The variations of these parameters were also studied as a function of the temperature T, the pressure P and the amount x of chromium in $Cr_xAl_{2-x}O_3$ (Poole 1964; Poole and Itzel 1963). Starting from the idea that the crystal field Δ and the Racah parameter B depend only on the Cr–O distance, three different laws for their variations were found, depending on which parameter, T, P or x, was at the origin of the variation of the Cr–O distance. These results tend to prove that the value of the crystal field as measured by the $^4A_{2g} \rightarrow {}^4T_{2g}$ transition energy is not simply a function of the Cr–O distance. McClure (1962) studied the optical absorption spectra of ruby (Al_2O_3:Cr^{3+}) in detail. To interpret some features, he needed to consider complex models. He calculated the potential for a chromium impurity displaced by 0.1 Å toward or away from the nearest cation in the structure and proposed a tetragonal distortion of the excited state. These high-quality and detailed studies of Al_2O_3–Cr_2O_3 solid solution series were made within the virtual crystal approximation, in which the chromium atom is supposed to substitute exactly for the aluminum atom in the structure, so that the Cr–O distances in ruby are the same as the Al–O distances in α-Al_2O_3. This leads to mistakes and to misunderstandings. Actually, when chromium substitutes for aluminum, the chromium site is expected to be different from the aluminum site in α-Al_2O_3, due to the larger ionic radius of chromium ($r^{3+}_{Cr} = 0.615$ Å) compared to that of aluminum ($r^{3+}_{Al} = 0.535$ Å) in an octahedral site (Shannon 1976). As a consequence, the understanding of the local environment around the chromium atom is absolutely needed to explain the evolution of physical properties with respect to the chromium content x in $Cr_xAl_{2-x}O_3$.

Subsequently, many studies have been undertaken to determine the chromium site in ruby (α-Al_2O_3:Cr^{3+}). Single crystal X-ray diffraction (McCauley and Gibbs 1972; Moss and Newnham 1964), UV–VIS spectroscopy (McClure 1962; Langer 2001; Andrut et al. 2004) and EPR spectroscopy (Büscher et al. 1987) have shown the existence of relaxations around the chromium atom in α-Al_2O_3. Extended X-ray absorption fine structure (EXAFS) has been performed at the Cr K-edge on powders (Kizler et al. 1996) or single crystals (Emura et al. 1993) of ruby. In a previous piece of work, we determined Cr–O bond lengths in the coordination shell by linear dichroic EXAFS at the chromium K-edge in α-Al_2O_3:Cr^{3+} (Gaudry et al. 2003). However, to our knowledge, no EXAFS experiment has been undertaken on the whole Al_2O_3–Cr_2O_3 solid solution.

In a first step, we evaluate the influence of the crystal field Δ and the Racah parameter B on the colors of the green eskolaite and the red ruby. These two parameters are usually deduced from the positions of large features in the UV–VIS spectra, using a semi-quantitative theory. Our approach is to analyze the isotropic X-ray absorption spectra and the X-ray magnetic circular dichroic (XMCD) spectra at the Cr $L_{2,3}$-edges with the quantitative ligand field multiplet (LFM) theory following Theo Thole's developments (Cowan 1981; Butler 1981; Thole et al. 1985), in order to address the values of Δ and B from a different point of view. In addition, this analysis gives access to the nature of the Cr–O bonding in α-Cr_2O_3 and $Cr_{0.07}Al_{1.93}O_3$. To our knowledge, no X-ray absorption spectroscopy (XAS) at the Cr $L_{2,3}$-edges in $Cr_xAl_{2-x}O_4$ has yet been made. The structural environment around chromium in the whole solid solution Al_2O_3–Cr_2O_3 is also specified by XAS at the chromium K-edge. We especially focused on the determination of the mean Cr–O distances for several values of x in $Cr_xAl_{2-x}O_3$, in order to make a link between the color change and the local environment around chromium in the Al_2O_3–Cr_2O_3 series. Given that the same technique is used for the whole solid solution series, the results for different chromium concentrations are directly comparable.

Materials and methods

Synthesis of the samples

Corundum, α-Al_2O_3, and eskolaite, α-Cr_2O_3, belong to the $R\bar{3}2/c$ space group (Wyckoff 1964). They are a stacking of distorted octahedra made of six oxygen atoms, at the center of which lies an aluminum atom (in α-Al_2O_3) or a chromium atom (in α-Cr_2O_3). The six oxygen atoms are gathered into two groups of three atoms to comply with the C_3 local symmetry. These two groups lie at two different distances from the central atom. The nearest three oxygen atoms, labeled O_1, are between edge-shared octahedra and lie at 1.96 Å in α-Cr_2O_3 and 1.86 Å in α-Al_2O_3. The farther three oxygen atoms, labeled O_2, are between face-shared octahedra and lie at 2.01 Å in α-Cr_2O_3 and 1.97 Å in α-Al_2O_3. The closer Cr–Cr pairs in α-Cr_2O_3 lie at 2.65 Å (one pair) and 2.88 Å (three pairs), while the closer Al–Al pairs in α-Al_2O_3 lie at 2.65 Å (one pair) and 2.79 Å (three pairs) (Pearson 1962; Finger and Hazen 1980).

The $Al_{2-x}Cr_xO_3$ powders were prepared by co-precipitation and subsequent calcination (Bondioli et al. 2000). The amorphous gels of Al^{3+} and Cr^{3+} hydroxides were co-precipitated with ammonia (NH_4OH, RPE, Carlo Erba, Milan, Italy) from aluminum nitrate [$Al(NO_3)_3$, RPE, Carlo Erba] and chromium nitrate

[$Cr(NO_3)_3$, RPE, Carlo Erba] solutions at pH 9. The amorphous co-precipitated hydroxides, carefully washed with distilled water, were dried in a conventional furnace at 120°C and then ground in an agate mortar. The powders obtained were calcined in air, in an electric furnace, for 3 h at 1,300°C. All the heat-treated samples form a highly pure and crystalline solid solution, whatever the level of chromium content. The samples have been characterized by many techniques presented elsewhere (Bondioli et al. 2000).

X-ray absorption spectroscopy

Cr K-edge EXAFS

Fine powders of the $Al_{2-x}Cr_xO_3$ samples ($x = 2.00$, 1.00, 0.45, 0.29, 0.07) were mixed with cellulose and mounted on a sample holder for EXAFS data collection at beamline D44 of DCI storage ring at LURE (France). Spectra were collected at the Cr K-edge (5,989 eV) in transmission mode using a pair of Si(111) monochromator crystals. The beamline is equipped with a pair of borosilicate parallel mirrors working in specular reflection to reject harmonic reflections. The monochromator was calibrated by assigning an energy value of 5,989 eV to the first inflection point in the absorption edge of a Cr metal reference foil. Samples were mounted in a liquid nitrogen cryostat ($\simeq 77$ *K*) to decrease thermal disorder. Three spectra were collected for all samples except $Al_{1.93}Cr_{0.07}O_3$, for which ten spectra were registered. A standard procedure is used to extract the normalized EXAFS signal from the absorption spectra (Winterer 1997). The EXAFS spectra at the Cr K-edge of the five samples are shown in Fig. 1.

These normalized EXAFS signals at the Cr K-edge were further analyzed by two complementary methods. The contributions from oxygen shells in the coordination sphere were isolated and analyzed by a Fourier series of plane wavelets. The typical k range used to obtain the radial structure function in real space was 3.90–15.60 $Å^{-1}$. The EXAFS function was k^2-weighted. An appropriate r range was selected to separate the contributions of the nearer shells from the total experimental signal using back Fourier transform. Typically, the r range was 0.90–1.96 Å. EXAFS fitting was performed using the program EXAFS (Bonnin et al. 1985) with theoretical phases, amplitudes and mean free paths calculated with the FEFF8 code (Ankudinov et al. 1998). Starting models for these calculations included α-Cr_2O_3 and a structural model resulting from an ab initio energy minimization (see below). Four adjustable parameters (r_j, σ_j, N_j, ΔE_0^j) were fitted for one shell. The isotropic signal was analyzed with only one mean metal–oxygen distance for the fit, although the difference between the shorter Cr–O_1 and the longer Cr–O_2 distances should lead to two separate Cr–O distances. Indeed, this difference was expected to be less than 0.09 Å for both α-Cr_2O_3 and $Cr_{0.07}Al_{1.93}O_3$ (Pearson 1962; Gaudry et al. 2003), which would induce a beating effect on the spectra, with a first node for $2k\Delta r = \pi$, where $k = 18$ $Å^{-1}$ for $\Delta r = 0.09$ Å. Since our spectra were recorded on a shorter k range, this beating effect cannot be seen and the terms corresponding to the Cr–O_1 and Cr–O_2 shells can then be mixed together to give a single term corresponding to a mean Cr–O distance, with an additional contribution to σ_{static} (Teo 1985). This point has been extensively discussed in Fig. 5 of Gaudry et al. (2003). The σ_{static} values can be found in Table 1. As a second method, we applied a global simulation of $\chi(k)$ using structural models and calculation of the Cr K-edge (see below).

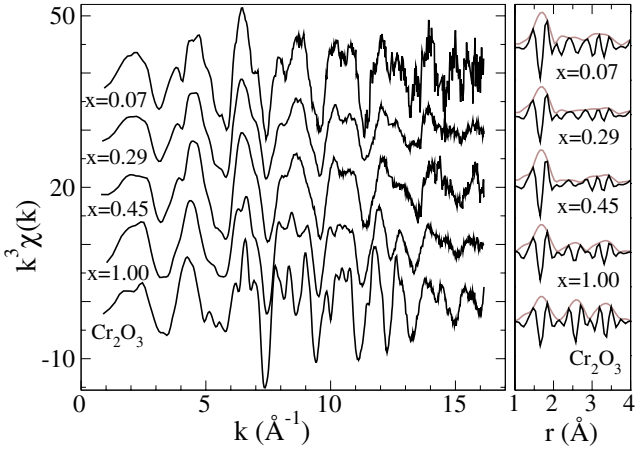

Fig. 1 EXAFS $k^3\chi(k)$ functions (*left*) and Fourier transforms (*right*) for the $Cr_xAl_{2-x}O_3$ powders ($x = 0.07$, 0.29, 0.45, 1.00, 2.00)

Cr $L_{2,3}$-edges

The experiments were carried out both at beamline ID8 of the European Synchrotron Radiation Facility (ESRF) in Grenoble (France) and at beamline SU23 of the Super-ACO storage ring at LURE in Orsay (France). On ID8 the photon source was an Apple II undulator that delivers a high flux of circularly polarized light with a polarization rate of about 100%. The monochromator was a Dragon type one with spherical grating. Isotropic and XMCD signals of sample $Cr_{0.07}Al_{1.93}O_3$ have been measured at ≈6 K in a magnetic induction of 7 T. On SU23 the photon source was an asymmetric wiggler that delivers a moderate flux of elliptically polarized light above and below the orbit plane of the storage ring. The polarization rate was estimated to be around 45%. The photons were monochromatized by a plane grating with fixed exit slit (Arrio et al. 1999). The isotropic cross-section has been measured at 4.2 K for Cr_2O_3 and for $Cr_{0.14}Al_{1.86}O_3$. XMCD on $Cr_{0.14}Al_{1.86}O_3$ has also been measured. The results concerning $Cr_{0.14}Al_{1.86}O_3$ are in line with those measured at ESRF on $Cr_{0.07}Al_{1.93}O_3$ and are not presented here. Since α-Cr_2O_3 is antiferromagnetic (Brown et al.

Table 1 Mean Cr–O distances in the coordination shell of chromium in the whole solid solution series Al_2O_3–Cr_2O_3

Sample	r (Å)	σ (Å)	N	ΔE_0 (eV)	GOF
Cr_2O_3	1.98_0	0.062	6.0	−3.0	0.006
$CrAlO_3$	1.97_0	0.059	5.6	−3.7	0.008
$Cr_{0.45}Al_{1.55}O_3$	1.96_5	0.052	6.4	−5.3	0.013
$Cr_{0.29}Al_{1.71}O_3$	1.96_5	0.057	5.7	−5.3	0.008
$Cr_{0.07}Al_{1.93}O_3$	1.96_5	0.051	6.4	−2.3	0.009

2002), its XMCD signal is zero. The spectra at the Cr $L_{2,3}$-edges are reported in Fig. 2.

Theoretical calculations

Cr K-edge

X-ray absorption spectra are calculated within a real space multiple scattering approach (FEFF8) for a *muffin-tin* potential with a screened core hole (Ankudinov et al. 1998). Structural models are validated by a direct comparison between the experimental and the calculated $k^3\chi(k)$. The structural model for α-Cr_2O_3 is a rhombohedral unit cell defined by $a = 5.35$ Å and $\alpha = 55.12°$ (Finger and Hazen 1980). The EXAFS signal for this structural model is computed for a cluster size of 6.3 Å around the absorbing atom. The total number of paths whose intensities are larger than 4% of the EXAFS contribution from the first three oxygen neighbors was found to be equal to 150. For all these paths, the number of legs was strictly less than six. The FEFF8 EXAFS curve was then multiplied by a broadening Gaussian function to take into account the Debye Waller broadening ($\sigma = 0.06$ Å). The structural model for $Cr_{0.07}Al_{1.93}O_3$ is given by an ab initio energy minimization using the density functional theory and the spin polarized local density approximation (Car and Parrinello 1985). The cell used in the density functional calculations is a super-cell built on the vectors $2\vec{a}_R, 2\vec{b}_R, 2\vec{c}_R$ ($\vec{a}_R, \vec{b}_R, \vec{c}_R$ are the base vectors of the rhombohedral unit cell) and contained 80 atoms as follows: 1 chromium atom, 31 aluminum atoms and 48 oxygen atoms. The lattice constants are those resulting from the calculation of reference (Duan et al. 1998): $a_R = 5.11$ Å and $\theta = 55.41°$. The super-cell is large enough to minimize interaction between two paramagnetic ions: the minimum distance between two of these is 10.22 Å. The spin multiplet degeneracy imposed on the trivalent paramagnetic ions is four for Cr^{3+}. The calculations are performed with the cpmd program (Hutter et al. 1996). From this structural model, a theoretical EXAFS was calculated by the FEFF8 code. For this calculation, we used the same set of parameters as those detailed for Cr_2O_3 except for the Debye Waller factor that we choose equal to $\sigma = 0.04$ Å.

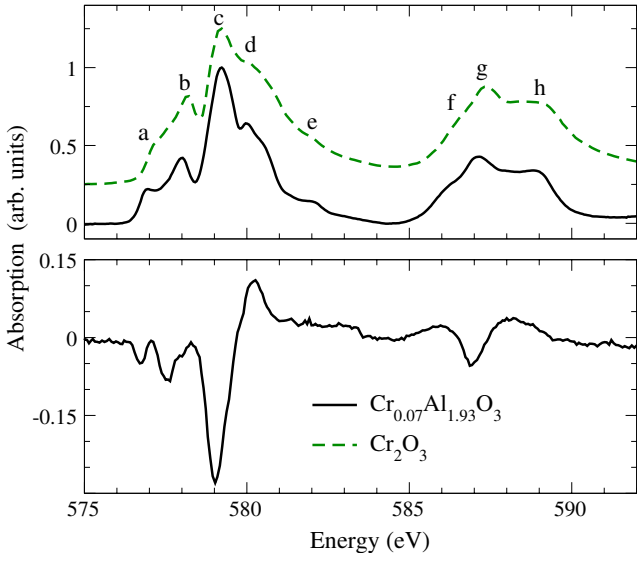

Fig. 2 Isotropic (*top*) and XMCD (*bottom*) spectra at the Cr $L_{2,3}$-edge in α-Cr_2O_3 (*dashed line*) and $Cr_{0.07}Al_{1.93}O_3$ (*solid lines*). The spectra are normalized to 1.0 at the maximum of the isotropic L_3-edge

Cr $L_{2,3}$-edges: ligand field multiplet calculations

The $L_{2,3}$-edges are analyzed with the LFM calculations. These calculations describe the transition for a single chromium ion in a given symmetry, from a $2p^63d^3$ ground state to a $2p^53d^4$ excited state (Cowan 1981; Butler 1981; Thole et al. 1985). The calculation is parameterized. The parameters are adjusted to minimize the differences between the calculated and the experimental spectra. Coulomb interactions, exchange interactions and 2p and 3d spin–orbit interactions in the initial (F^2_{dd}, F^4_{dd}, ζ_{3d}) and final states (F^2_{dd}, F^4_{dd}, F^2_{pd}, G^1_{pd}, G^3_{pd}, ζ_{2p}, ζ_{3d}) are calculated in the spherical symmetry. The electron–electron interactions are reduced by a factor labeled κ_X that takes into account effects such as covalency and charge transfer. All electron–electron integrals are reduced by the same factor. Although the local Cr^{3+} site symmetry in α-Cr_2O_3 is a slightly distorted octahedron (C_3 symmetry), with three Cr–O distances of 1.96 Å and three Cr–O distances of 2.01 Å (Finger and Hazen 1980), we described the local symmetry of the chromium site in $Cr_xAl_{2-x}O_3$ by O_h. In fact, the isotropic absorption spectrum does not depend on such small distortions (Theil et al. 1999). In O_h symmetry, the monoelectronic 3d level is split into e_g and t_{2g}. The energy separation between these two states is the crystal field parameter, labeled $\Delta_X = \epsilon_{e_g} - \epsilon_{t_{2g}}$, for the X-ray energy range. For LFM calculation applied to $L_{2,3}$-edges, one is dealing with transitions between $2p^63d^3$ toward $2p^53d^4$. One then needs two sets of parameters for the initial and the final states. The initial states parameters are set to the values obtained by UV–VIS spectroscopy, i.e., $\Delta = 2.24$ eV (18,070 cm^{-1}) and $B = (9F^2 - 5F^4)/441 = 0.080$ eV (645 cm^{-1}) for $Cr_{0.07}Al_{1.93}O_3$ and $\Delta = 2.07$ eV (16,700 cm^{-1}) and

$B = 0.058$ eV (468 cm^{-1}) for α-Cr_2O_3. In fact we checked that the LFM calculations do not depend much on the parameters for the initial state ($2p^63d^3$). On the contrary the set of parameters Δ_X and B_X for the final state ($2p^53d^4$) strongly modifies the intensities and energies of the transitions. One then proceeds to a fit between experiment and calculations to determine the set of parameters for the final state. They are not expected to be exactly identical to those found from UV–VIS spectroscopy, due to the 2p core hole. The broadening of the line spectrum is determined by the lifetime of the final states and is mainly determined by Auger decay from this final state ($2p^53d^4$). The relaxation rate of each individual final state is unknown. Individual spectral features and shoulders can have different broadening factors. The calculated spectra are broadened using a Lorentzian with a 2Γ full width at half maximum (FWHM), with $2\Gamma = 0.2$ eV (L_3) and $2\Gamma = 0.6$ eV (L_2) and convoluted with a Gaussian with 0.5 eV FWHM, to describe the total lifetime and instrumental broadening processes.

In the UV–VIS range, the LFM calculations are also used to evaluate the dependence of various band energies of chromium in the $2p^63d^3$ initial state ($^4T_{1g}$, $^2T_{2g}$, $^4T_{2g}$, $^2T_{1g}$, $^2E_{1g}$) as a function of Δ/B.

Results and discussion

Our ultimate purpose is to connect the green color of eskolaite (α-Cr_2O_3) and the red color of ruby (α-Al_2O_3:Cr^{3+}) to the local organization around chromium. To do so, it is worth knowing the effects of the structural and electronic parameters around chromium on the positions of the transmission and absorption bands.

Color and band energies in $Cr_xAl_{2-x}O_3$

In this part, LFM calculations are performed to (1) evaluate the contributions of the electronic parameters Δ and B on the positions of the UV–VIS transmission bands of α-Cr_2O_3 and $Cr_{0.07}Al_{1.93}O_3$ and (2) interpret the X-ray absorption spectra at the $L_{2,3}$-edges in α-Cr_2O_3 and $Cr_{0.07}Al_{1.93}O_3$.

Band energies

The colors of eskolaite and ruby are mainly due to the positions of the transmission bands. One of them lies approximately at the middle of the two absorption bands of energies ε_1 and ε_2. When one affirms that the position of the transmission band is given by $\epsilon_m = (\epsilon_1 + \epsilon_2)/2$, one makes the assumption that the transitions $^4A_{2g}(O_h)$ towards $^4T_{2g}(O_h)$ and $^4A_{2g}(O_h)$ towards $^4T_{1g}(O_h)$ have similar intensities and similar widths for powders. The difference of the exact position of the transmission maximum with our estimation ε_m of the transmission maximum is evaluated to be around 0.025 eV (200 cm^{-1}).

We evaluate the dependence of $\epsilon_m = (\epsilon_1 + \epsilon_2)/2$ and $\varepsilon_d = \varepsilon_1 - \varepsilon_2$ by multiplet calculations, taking into account the spin–orbit coupling and the trigonal distortion of the chromium site. We performed the calculation with spin–orbit coupling and trigonal distortion to see how the splittings due to these effects would spread the various transitions. The trigonal distortion arises from the fact that in M_2O_3 compounds, the metallic atom (M) lies in a C_3 symmetry site (Hahn 1995). However, it is allowed to treat it as if it were C_{3v} in the absence of external magnetic field (Sugano and Tanabe 1958). In C_{3v} symmetry, the $^4A_{2g}(O_h)$ spectroscopic term becomes $^4A_2(C_{3v})$, while the $^4T_{2g}(O_h)$ spectroscopic term is split into $^4E(C_{3v})$ and $^4A_1(C_{3v})$ and the $^4T_{1g}(O_h)$ spectroscopic term is split into $^4E(C_{3v})$ and $^4A_2(C_{3v})$. So, for the trigonal splitting, we introduced a C_{3v} distortion yielding the experimentally observed splittings on the $^4T_{2g}(O_h)$ and $^4T_{1g}(O_h)$ levels. Spin–orbit coupling on the 3d level was extracted from atomic calculations ($\zeta_{3d} = 35$ meV). The various levels above the ground state are reported in Fig. 3. We do not consider the negligible $^4A_{2g}(O_h)$ ground-state splitting (< 0.08 meV). From Fig. 3, one notices that the energy spread for $^4T_{2g}(O_h)$ levels is quite large. For the particular set of parameters of α-Cr_2O_3, the $^4T_{2g}(O_h)$ and $^2T_{2g}(O_h)$ states can hybridize efficiently. This means that the ε_1 transition cannot be assigned to the single transition $^4A_{2g}(O_h)$ toward $^4T_{2g}(O_h)$ any more, but rather to a set of nine different transitions spread around 125 meV (≈1,000 cm^{-1}, 6% of Δ).

From LFM calculation, the variations $d\varepsilon_m$ of ε_m and $d\varepsilon_d$ of ε_d as functions of the variations $d\Delta$ of Δ and dB of B are

$$d\epsilon_m \simeq 4.2\,dB + 1.02d\Delta \tag{1}$$

and

$$d\epsilon_d \simeq 8.5\,dB + 0.057\frac{B}{0.068\,(\text{eV})}d\Delta. \tag{2}$$

Since the parameter Δ ranges from 2.24 eV (18,070 cm^{-1}) in ruby to 2.07 eV (16,700 cm^{-1}) in eskolaite and the Racah parameter B from 0.080 eV (645 cm^{-1}) in ruby to 0.058 eV (468 cm^{-1}) in eskolaite (Reinen 1969), 35% of the variation of ε_m is due to the variation of B and the remaining 65% to the variation of Δ, while the variation of ε_d is mainly due to the variation of B (95%). The spin–orbit coupling and the trigonal distortion lead to a broadening of the states. For example, due to spin–orbit coupling, the $^4T_{2g}(O_h)$ is mixed with the $^2T_{2g}(O_h)$. The broadness of these bands can be greater than the range of variation of one state as a function of x in the whole $Cr_xAl_{2-x}O_3$ composition.

The covalence of the Cr–O bonding (Racah parameter B) efficiently conditions the color (35%). The analysis of the X-ray absorption spectra at the $L_{2,3}$-edges is then meaningful because this technique is a probe for

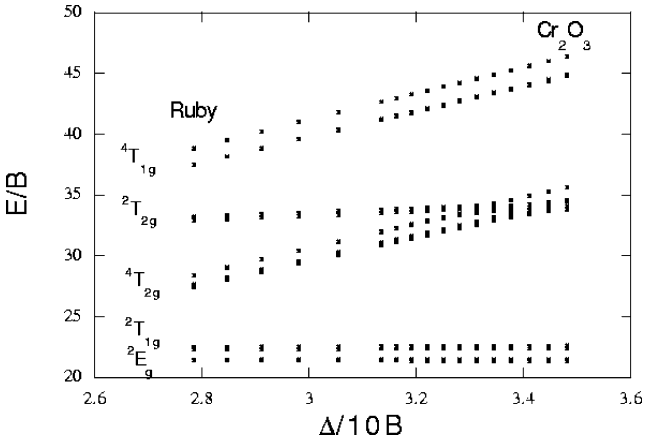

Fig. 3 Variations of the ratio E/B, where E is the energy of various bands ($^4T_{1g}$, $^2T_{2g}$, $^4T_{2g}$, $^2T_{1g}$, ^2E_g in O_h symmetry), as a function of $\Delta/10B$. From UV–VIS spectroscopy, $\Delta/10B = 3.475$ for Cr_2O_3, and $\Delta/10B = 2.784$ for ruby

the 3d orbitals that are effective in the appearance of coloration.

XAS at the Cr $L_{2,3}$-edges

The isotropic signal of the α-Cr_2O_3 and the $Cr_{0.07}Al_{1.93}O_3$ samples are quite identical because they are the signature of a Cr^{3+} ion with the $3d^3$ ionic configuration in an octahedral environment (Fig. 2). Eight similar features appear on the spectra of both samples. However, the positions and intensities of some of them are different. The difference $E_g - E_c$ between the c (L_3-edge) and g (L_2-edge) features is 8.2 eV for α-Cr_2O_3 while it is 7.9 eV for $Cr_{0.07}Al_{1.93}O_3$. The difference $E_b - E_c$ between the b and c features of the L_3-edge is larger (1.20 eV) for $Cr_{0.07}Al_{1.93}O_3$ than it is for α-Cr_2O_3 (1.05 eV). The position and the shape of peak a is different for the two samples. These isotropic $L_{2,3}$-edges can be analyzed with LFM calculations.

We are interested in the determination of two parameters, namely Δ_X and B_X. The last parameter is closely linked to the κ_X parameter by $\kappa_X = B_X/B_X^0$ where B_X^0 is the calculated Racah parameter for the free ion ($B_X^0 = 0.154$ eV). From the optical spectra of free ions and extrapolation, Sugano and Tanabe (1958) give $B^0 = 0.114$ eV. The theoretical B_X^0 and experimental B^0 values differ, due to the presence of the 2p core hole in the X-ray range. For the isotropic signals, it is worth noticing that when the parameter Δ_X increases, the peak a appears progressively. When the parameter κ_X increases, the peak a disappears steadily, the peak b is displaced toward lower energies and increases in intensity. To have a precise idea of the influence of the Δ_X and κ_X parameters on the position of the b feature, we have plotted the difference $E_c - E_b$ between the calculated b and c features for different values of Δ_X and κ_X (see Fig. 4). The difference $E_c - E_b$ is almost independent of the Δ_X parameter for a given value of κ_X in the energy range 1.6–2.2 eV, but it increases steadily with the κ_X parameter, for a given value of Δ_X. It is then possible to determine the κ_X value from the experimental value of $E_c - E_b$, which is about 1.05 eV for α-Cr_2O_3 and 1.20 eV for $Cr_{0.07}Al_{1.93}O_3$. It implies a κ_X value of 0.55 for α-Cr_2O_3 and 0.65 for $Cr_{0.07}Al_{1.93}O_3$. The Δ_X value is determined by the shape of the spectra, in particular by the relative intensity of the a feature. Therefore, we have compared the calculated and experimental Cr $L_{2,3}$-edges. The calculations were made for 14 different values of Δ_X, in the range 1.5–2.8 eV, with either $\kappa_X = 0.65$ or $\kappa_X = 0.55$. From all these calculations, we deduce $\Delta_X(\alpha\text{-}Cr_2O_3) = 1.8$ eV and $\Delta_X(Cr_{0.07}Al_{1.93}O_3) = 2.1$ eV. The dichroic signal provides useful information on these parameters too. It is worth noticing that when the Δ_X parameter increases, the I_a/I_b ratio increases, where I_a and I_b are the intensities of peak a and b, respectively (the labeling of the spectral features is defined in Fig. 2), while when the κ_X parameter increases, the I_a/I_b ratio decreases. In addition, the difference $E_c - E_b$ is almost independent of the variation of the Δ_X parameter, while it increases with the κ_X parameter. Similar to the isotropic signals analysis, we can deduce values of κ_X and Δ_X that agree with the previous values. This corroborates the previous Δ_X and κ_X parameters for $Cr_{0.07}Al_{1.93}O_3$.

We have plotted in Fig. 5 the final fit of our data. The parameters used for the Cr^{3+} ($2p^53d^4$) final configuration are $\Delta_X = 2.1$ eV (16,940 cm^{-1}), $\kappa_X = 0.65$, $\zeta_{2p} = 5.902$ eV and $\zeta_{3d} = 0.047$ eV for $Cr_{0.07}Al_{1.93}O_3$, and $\Delta_X = 1.8$ eV (14,520 cm^{-1}), $\kappa_X = 0.55$, $\zeta_{2p} = 6.034$ eV and $\zeta_{3d} = 0.047$ eV for α-Cr_2O_3. The Racah parameter B_X deduced from κ_X is greater in $Cr_{0.07}Al_{1.93}O_3$ (0.100 eV) than in eskolaite (0.085 eV). The crystal field Δ_X is greater in $Cr_{0.07}Al_{1.93}O_3$ (2.1 eV) than in eskolaite (1.8 eV). These results are in line with the ones given by UV–VIS spectroscopy, which are $\Delta = 2.24$ eV (18,070 cm^{-1}) for ruby and $\Delta = 2.07$ eV (16,700 cm^{-1}) for eskolaite and $B = 0.080$ eV (645 cm^{-1}) for ruby and $B = 0.058$ eV (468 cm^{-1}) for eskolaite. From the fitting procedure, one sees that Δ_X varies by +15% between α-Cr_2O_3 and $Cr_{0.07}Al_{1.93}O_3$ and B_X by +17%. This is the same general trend as the one observed in UV–VIS spectroscopy. Indeed, the crystal field Δ increases by about +8% when the concentration x decreases from 2 to 0, while variation of the Racah parameter B is +32% (Reinen 1969). However, the values of the variations of the amplitudes given by UV–VIS spectroscopy or XAS are different. This difference is related to the fact that the parameters Δ_X and B_X are by definition different from Δ and B, due to the 2p core hole.

Color and structural environment around Cr in $Cr_xAl_{2-x}O_3$

Since the variation of ε_m, causing the green color of α-Cr_2O_3 and the red color of ruby, is mainly due to the variation of the crystal field Δ (65%), we examine in the

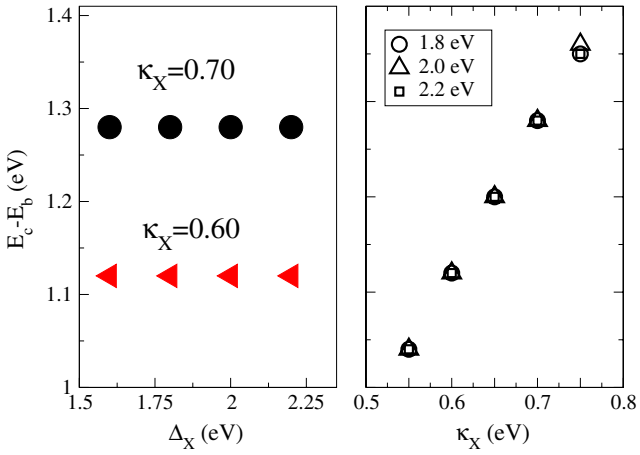

Fig. 4 Influence of the Δ_X and κ_X parameters on the difference $E_c - E_b$ between the features b and c of the calculated isotropic absorption spectra at the Cr $L_{2,3}$-edges

following whether the only variation of the Cr–O distance in the solid solution series can explain the variation of Δ.

XAS at the Cr K-edge

The EXAFS functions of the five samples are shown in Fig. 1 (left panel). The spectra of α-Cr_2O_3 and $Cr_{0.07}Al_{1.93}O_3$, the two poles of the solid Al_2O_3–Cr_2O_3 solid solution, are very different from each other, suggesting a different local environment for chromium atoms in both structures. The spectra of α-Cr_2O_3 contains more features. In the k range 5-13 Å^{-1}, characteristic features disappear steadily from α-Cr_2O_3 to $Cr_{0.07}Al_{1.93}O_3$. For instance, the three sharp features at about 8–9 Å^{-1}, which are present in the spectra of α-Cr_2O_3, become two features in the spectra of $Cr_{0.07}Al_{1.93}O_3$. It is the same for the three features at about 6–7 Å^{-1} on the spectra of α-Cr_2O_3. The FEFF8 calculations show that these EXAFS features are mainly due to single Cr–Cr scattering paths (up to 6 Å) in α-Cr_2O_3. The substitution of chromium atoms by Al atoms from α-Cr_2O_3 to $Cr_{0.07}Al_{1.93}O_3$ could explain the disappearance of these features, because aluminum atoms have lower back-scattering amplitude than chromium atoms. However, structural changes between α-Cr_2O_3 and $Cr_{0.07}Al_{1.93}O_3$ could also explain the changes observed in EXAFS spectra. On Fig. 1 (left panel), one notices that there is a continuous change of the Cr K-edge X-ray absorption signals from α-Cr_2O_3 to $Cr_{0.07}Al_{1.93}O_3$. An attempt to fit EXAFS spectra for intermediate composition with a linear combination of the EXAFS spectra of the two poles (α-Cr_2O_3 and $Cr_{0.07}Al_{1.93}O_3$) by a least square fitting procedure failed. This result indicates that the local environment around chromium in $Cr_xAl_{2-x}O_3$ is not a ponderated average of chromium environment in $Cr_{0.07}Al_{1.93}O_3$ and Cr_2O_3. This result can be interpreted as continuous modification of chromium environment within the series. It also shows that there is no chromium clustering in the samples, in agreement with previous work (Bondioli et al. 2000). The first peak of the Fourier transform that contains the contributions of two Cr–O pairs, with quite similar Cr–O distances, is comparable from α-Cr_2O_3 to $Cr_{0.07}Al_{1.93}O_3$, suggesting that there is no significant structural change in the chromium coordination sphere in the whole range Cr_2O_3–Al_2O_3. From α-Cr_2O_3 to $CrAlO_3$, the other peaks are very similar (Fig. 1, right panel), but their intensity decreases considerably. This decrease would be due to the increase of aluminum concentration from α-Cr_2O_3 to $CrAlO_3$. This hypothesis is supported by the canceling of the Cr–Cr and Cr–Al pairs contributions, shown in Fig. 6. In $Cr_{0.45}Al_{1.55}O_3$ and $Cr_{0.29}Al_{1.71}O_3$, the intensities of the second and third peaks in the Fourier transform are almost null. The canceling of the Cr–Cr and Cr–Al pairs contributions is added to a probably large spreading of bonds lengths in the structure. In $Cr_{0.07}Al_{1.93}O_3$, the second peak in the Fourier transform increases. The structure around chromium becomes again enough organized, but in a different way as that occurred in the α-Cr_2O_3 structure.

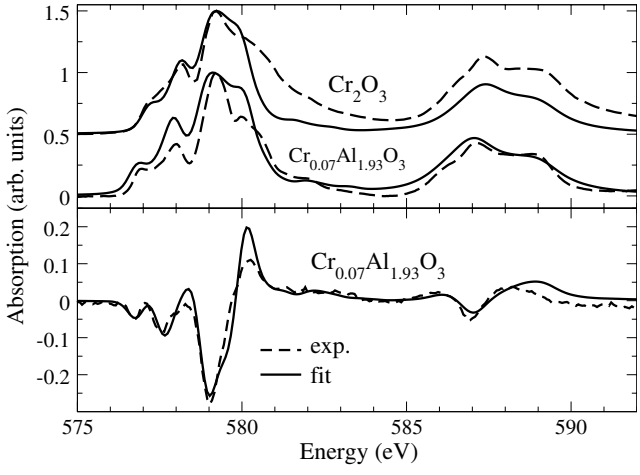

Fig. 5 Fitted isotropic and dichroic spectra of Cr_2O_3 and $Cr_{0.07}Al_{1.93}O_3$. The *straight line* is the fit and the *dashed line* is the experimental spectra (see text for calculation parameters)

The local environment of chromium in the Al_2O_3–Cr_2O_3 solid solution series is specified by the EXAFS analysis. The results for the first shell are presented in Table 1. The parameter ΔE_0 can be different for each sample and for each shell, because it depends on electronic effects of the chemical bond taken into account (Teo 1985). The influence of this parameter on the final Cr–O distance was checked by fitting the Cr_2O_3 first shell with a mean Cr–O distance set at 1.98_0 Å and with various fixed values for ΔE_0. Results indicate that the variation of the goodness of fit for each fit, defined as

$$\xi^2 = \sum \left(\frac{k^3 \chi_{\text{exp}}}{\sqrt{\sum k^6 \chi_{\text{exp}}^2}} - \frac{k^3 \chi_{\text{fit}}}{\sqrt{\sum k^6 \chi_{\text{exp}}^2}} \right)^2 ,$$

is lower than 0.01 for $-5 \leq \Delta E_0 \leq 0$ (Fig. 7, right). The influence of ΔE_0 on the final Cr–O distance is then negligible. In the same way, the error on the mean Cr–O distance was evaluated by fitting the Cr_2O_3 first shell with ΔE_0 set at -1 eV and with various fixed values for the mean Cr–O distance. Results indicate that a majoration of 0.005 Å for the mean Cr–O distance yields a degradation of ≈100% for the goodness of fit (Fig. 7, left). Considering these results, the relative precision on the mean Cr–O distances can be estimated to be 0.005 Å for the whole series.

Concerning the α-Cr_2O_3 pole, the mean Cr–O distance (1.98_0 Å) is in good agreement with the one (1.98_5 Å) given by Finger and Hazen (1980). Concerning the $Cr_{0.07}Al_{1.93}O_3$ pole, our mean Cr–O distance (1.96_5 Å) is similar to EXAFS results on powders (1.96 Å) given by Kizler et al. (1996) and from optical spectra (1.96 Å) given by Langer (2001). It is larger than the one (1.95 Å) given by Andrut (2004) from the application of the superposition model to optical absorption data. Our mean Cr–O distance is also similar to the one (1.97 Å) determined from a previous work on single crystals (Gaudry et al. 2003). The EXAFS analysis shows that the average Cr–O bond length in $Cr_xAl_{2-x}O_3$ ($0.07 \leq x < 2$) increases by ≈1% in the whole Al_2O_3–Cr_2O_3 series (Fig. 8). This average Cr–O distance in $Cr_xAl_{2-x}O_3$ is close to the mean Cr–O distance in α-Cr_2O_3: 1.98_0 Å from this EXAFS study or 1.98_5 Å from Finger and Hazen (1980). It is longer than the averaged Al–O bond (1.91_5 Å) in α-Al_2O_3 in the whole range Al_2O_3–Cr_2O_3. Such a behavior matches the Pauling (1967) model. The relaxation parameter

$$\zeta = \frac{R_{Cr-O}(Cr_{0.07}Al_{1.93}O_3) - R_{Al-O}(Al_2O_3)}{R_{Cr-O}(Cr_2O_3) - R_{Al-O}(Al_2O_3)}$$

defined by Martins and Zunger (1984) is equal to ≈0.76. This is less than the value found for Co(II), Zn(II), Pb(II) or Mn(II) in calcite (0.8–0.9) (Reeder et al. 1999; Lee et al. 2002). It is also less than the ones found for S or Se in CdS_xSe_{1-x} (0.87–0.88) (Levelut et al. 1991). The ζ value for $Cr_{0.07}Al_{1.93}O_3$ is, however, larger than $\zeta = 0.5$ in FeO–MgO solid solutions (Waychunas et al. 1994) and values found by studies on alkali halide solid solutions lying between 0.4 and 0.6 (Martins and Zunger 1984; Boyce and Mikkelsen 1985; Frenkel et al. 1996). Actually, the corundum structure is made of edge and face-sharing octahedra that allow less flexibility than the corner-sharing octahedra structure of calcite, but more flexibility than the compact rock salt structure of MgO, FeO and alkali halide solid solutions.

For α-Cr_2O_3, the structure from Finger and Hazen (1980) allowed the calculation of the $\chi(k)$ signal for a chromium atom in such a crystal. This is compared in the upper part of Fig. 9 with the raw (non-Fourier filtered) experimental $\chi(k)$ signal. For the $Cr_{0.07}Al_{1.93}O_3$ sample, the structural model is built as follows: a 6.3 Å diameter cluster around chromium is determined from the ab initio energy minimization calculation, except for the average Cr–O distance of the chromium coordination shell, which is reduced by 0.5% to rescale it to the one found from isotropic EXAFS analysis (1.96_5 Å). The lower part of Fig. 9 shows that this model for $Cr_{0.07}Al_{1.93}O_3$ is consistent with the experimental $\chi(k)$ signal. It can be noticed that the FEFF8 EXAFS calculation without this Cr–O rescaling yields the same features as those in Fig. 9 (lower panel).

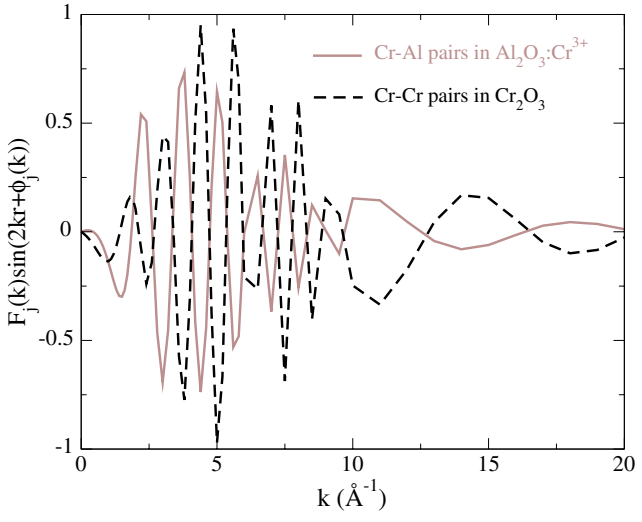

Fig. 6 $F_j(k)$ sin $(2kr + \Phi_j(k))$ functions for Cr–Cr pairs in α-Cr_2O_3 and for Cr–Al pairs in the structural model of ruby for the distance $r = 2.85$ Å

Influence of the Cr–O bonding on the crystal field

Since we determined how the variation of Δ induces the color change, we now turn to the question of the relationship between the variation of the Cr–O distance with the variation of Δ. In the point charge model, the dependence of the crystal field Δ on the mean metal–ligand distance is given by

$$\Delta = \frac{5}{3} Z_L e^2 \langle r^4 \rangle R_{Cr-O}^{-5}, \quad (3)$$

where R_{Cr}–O is the mean Cr–O distance, Z_L e^2 the effective charge of the ligands and $\langle r^4 \rangle = \int r^2 \, dr \, R_2(r)^2 r^4$, where $R_2(r)$ is the radial part of the d orbitals (Dunn et al. 1965). According to Langer (2001), the quantities Z_L e^2 and $\langle r^4 \rangle$ would be constant along the Al_2O_3–Cr_2O_3 solid solution series, because chromium lies in the same kind of site, with the same oxygen ligands in the whole range. Equation 3 is then rewritten as

$$\Delta = a R_{Cr-O}^{-5}, \quad (4)$$

where a is a constant. As shown from the EXAFS analysis at the Cr K-edge, the variation of the Cr–O distance in the whole composition range is ≈1%, while it is 8% for the Δ crystal field. According to Eq. 4, a variation of the Cr–O distance by 1.6% (more than 0.03 Å) would be necessary to explain the variation of Δ

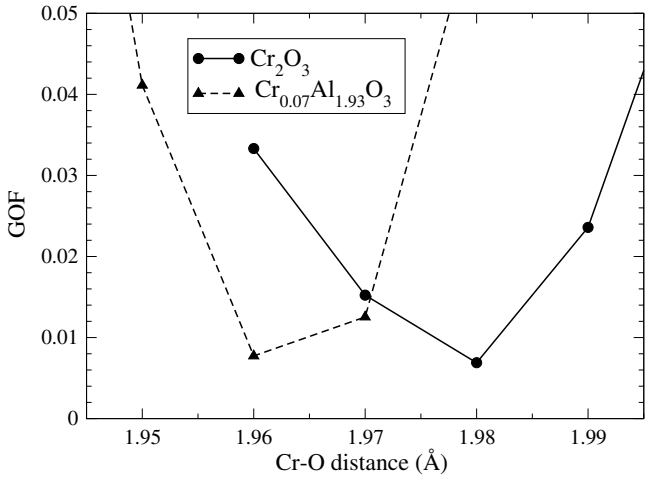

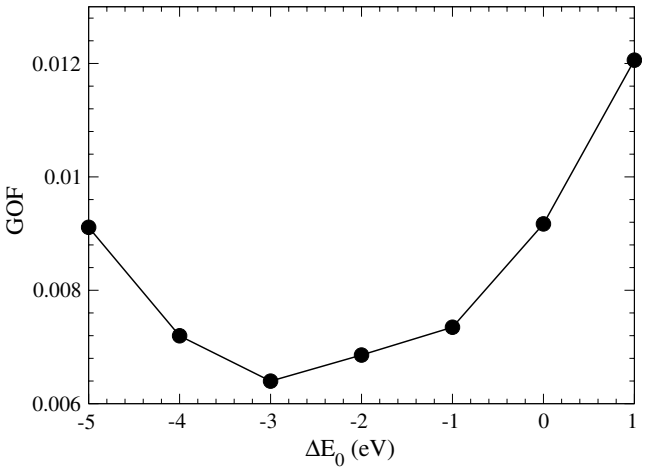

Fig. 7 *Left panel* variation of the goodness of fit (GOF) as a function of the Cr–O distance (ΔE_0 is fixed with $\Delta E_0 = -1.0$ eV) in α-Cr_2O_3 and $Cr_{0.07}Al_{1.93}O_3$. *Right panel* variation of the goodness of fit as a function of the ΔE_0 parameter in α-Cr_2O_3 (the Cr–O bond length is 1.98 Å)

(8% in the Al_2O_3–Cr_2O_3 series). This variation of the Cr–O distance is much larger than the one found (0.01_5 Å), which indicates that the variation of the mean Cr–O distance is not the only explanation for the variation of Δ. A different metal–ligand charge transfer between α-Cr_2O_3 and ruby probably occurs, so that a is no longer a constant in the whole solid solution series. The different metal–ligand charge transfer between α-Cr_2O_3 and ruby might be responsible for some percent in the variation of the crystal field. This statement is in agreement with the smaller value for the Racah parameter B in eskolaite than in ruby, and with the theory of Sugano and Peter (1961), for which the energy of the ${}^4A_{2g} \rightarrow {}^4T_{2g}$ transition is $\Delta + 10\xi B$, where ξ is a covalency parameter that stands for the different charge transfer between $\sigma(e_g)$ and $\pi(t_{2g})$ Cr–O bonds. The greater Cr–O bonding covalency in α-Cr_2O_3 than in α-Al_2O_3:Cr^{3+} comes from a modification of the electrostatic repulsions, and to configuration interaction. This means that the ground state of the chromium atom is described by the configuration $2p^63d^3$ interacting with $2p^63d^4\underline{L}$ where $\underline{L}$ represents a hole on a ligand.

Recent publications (Andrut et al. 2004; Brik et al. 2004) suggested that the variations of Δ was not strictly given by Eq. 4. Through a fitting procedure, Andrut et al. found that the exponent in Eq. 4 was in between 5 and 7.1, depending on the crystal host. By adding to the point charge model a contribution coming from both the covalent bond formation and the exchange interaction, Brik et al. found that the exponent was strictly larger than 5. On the other hand, Duclos et al. found that the pressure dependence of the Δ parameter was well described by $\Delta \propto V^{-5/3}$ (Duclos et al. 1990) in the short

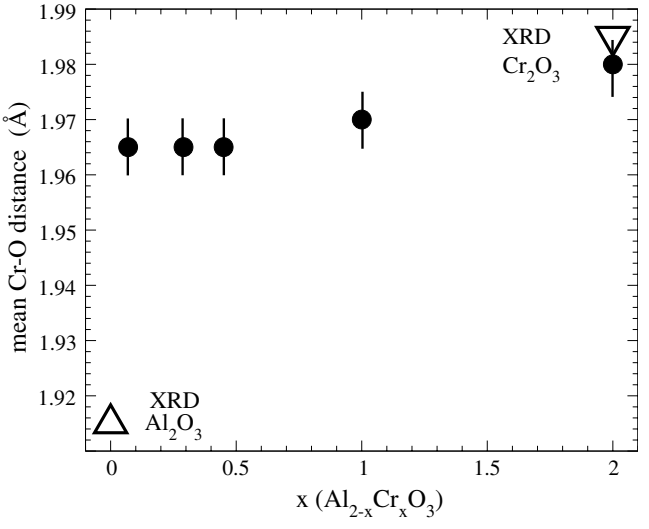

Fig. 8 Mean Cr–O distances (Å) from EXAFS analysis on $Cr_xAl_{2-x}O_3$ powders. *Black dots* are experimental points deduced from this study. *Triangles* are XRD data from Finger and Hazen (1980) and from Pearson (1962)

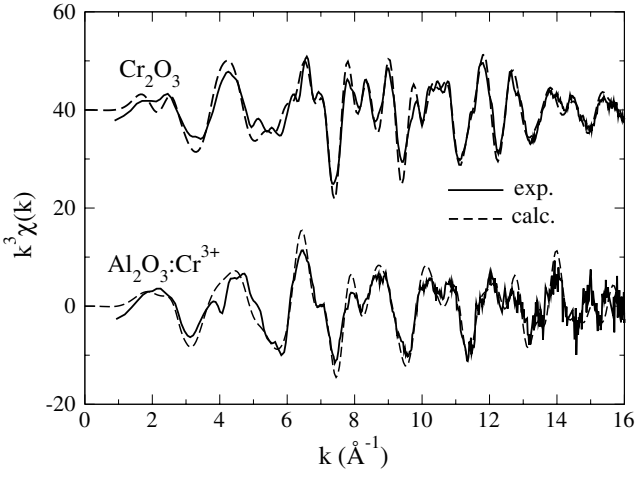

Fig. 9 The k^3-weighted experimental EXAFS (*solid lines*) and theoretical EXAFS (*dashed line*) for both the α-Cr_2O_3 and the α-Al_2O_3:Cr^{3+} structural models. Isotropic signals at Cr K-edge

range of pressure between 0 and 35 GPa. If for such moderate pressure, the unit cell volume is scaling as the cube of the averaged Cr–O distance, then Eq. 4 would be strictly obeyed. These pressure-dependent results are in line with those already published by Poole et al. (Poole 1964; Poole and Itzel 1963). These various findings can be harmonized in the following unifying picture. When one is comparing small variations of Δ parameter without changing the crystal host or the impurity concentration, the point charge model (i.e., Eq. 4) might be valid. When one is comparing variations of Δ due to changes of lattice host or impurity concentration, then the point charge model is clearly not sufficient and the theory needs to be modified to take into account the drastic chemical modifications around the impurity.

Conclusion

This study indicates that the color of the red ruby and the green eskolaite is partially due to both the crystal field and the covalence of the Cr–O bonding. In fact, the position of the transmission band is due 65% to the Δ value and 35% to the Racah B value. The variation in Cr–O distances from α-Cr_2O_3 to $Cr_{0.07}Al_{1.93}O_3$ estimated in this work is 0.01_5 Å (≈1%). It is too low to explain the variation of Δ in the point charge model. Following Sugano and Peter (1961), the variation of Δ could also be ascribed to the increase of the covalence of the Cr–O bond. Indeed, the Cr–Cr coupling in α-Cr_2O_3 might play a role in the covalence of the Cr–O bond by broadening the 3d band.

The study of the origin of the difference of color between the green emerald and the red ruby would be interesting. The Cr–O distances in ruby and emerald are probably close, the concentration of chromium is quite identical and very low in both minerals, so that no Cr–Cr coupling is expected to interfere with the color appearance. Such a study would be able to separate covalency effects from crystal field ones.

Acknowledgements We acknowledge the critical reading of the manuscript by Christian Brouder during its preparation. We thank Sandrine Brice-Profeta and Valérie Briois for fruitful discussions. We are very grateful to Mayeul d'Avezac for a careful reading of the manuscript. We are glad to thank the SU23 staff at LURE and the ID8 staff at ESRF for their skillful help during experiments. Computing time was partially supplied by the "Institut du Développement et des Ressources en Informatique Scientifique".

References

Andrut M, Wildner M, Rudowicz CZ (2004) EMU notes in mineralogy, vol 6, chapter 4. EOTVOS University press, pp 145–188

Ankudinov AL, Ravel B, Rehr JJ, Conradson SD (1998) Real space multiple scattering calculation and interpretation of X-ray absorption near edge structure. Phys Rev B 58:7565

Arrio M-A, Scuiller A, Sainctavit Ph, Cartier dit Moulin Ch, Mallah T, Verdager M (1999) Soft X-ray magnetic circular dichroism in paramagnetic systems: element-specific magnetization of two heptanuclear $Cr^{III}M_6^{II}$ high spin molecules. J Am Chem Soc 121:6414–6420

Bondioli F, Ferrari AM, Leonelli C, Manfredini T (2000) Reaction mechanism in alumina/chromia (Al_2O_3–Cr_2O_3) solid solutions obtained by coprecipitation. J Am Ceram Soc 83(8):2036

Bonnin D, Calas G, Suquet H, Pezerat H (1985) Sites occupancy of Fe^{3+} in Garfield nontronite: a spectroscopic study. Phys Chem Miner 12:55

Boyce JB, Mikkelsen JCJ (1985) Local structure of ionic solid solutions: extended x-ray absorption fine-structure study. Phys Rev B 31:6903–6905

Brik MG, Avram NM, Avram CN (2004) Crystal field analysis of energy level structure of the Cr_2O_3 antiferromagnet. Solid State Commun 132:831–835

Brown P, Forsyth JB, Berna EL, Tasset F (2002) Determination of the magnetization distribution in Cr_2O_3 using spherical neutron polarimetry. J Phys Condens Matter 14:1957–1966

Burns RG (1993) Mineralogical applications of crystal field theory, 2nd edn. Cambridge topics in mineral physics and chemistry, vol 5. Cambridge University Press, Cambridge

Büscher R, Such KP, Lehmann G (1987) Local relaxations around Fe^{3+} and Cr^{3+} in Al sites in minerals. Phys Chem Miner 14:553–559

Butler PH (1981) Point group symmetry, applications, methods and tables. Plenum, New York

Car R, Parrinello M (1985) Unified approach for molecular dynamics and density-functional theory. Phys Rev Lett 55:2471–2473

Cowan RD (1981) The theory of atomic structure and spectra. University of California Press, Berkeley

Duan W, Wentzcovitch RM, Thomson KT (1998) First-principles study of high pressure alumina polymorphs. Phys Rev B 57(17):10363–10369

Duclos SJ, Vohra YK, Ruoff AL (1990) Pressure dependence of the $^4T_2$ and $^4T_1$ absorption bands of ruby to 35 GPa. Phys Rev B 41(8):5372–5380

Dunn T, McClure DS, Pearson RG (1965) Some aspects of crystal field theory. Harper and Row, New York

Emura S, Maeda H, Kuroda Y, Murata T (1993) Coordination of Cr^{3+} ion in α-Al_2O_3. Jpn J Appl Phys 32(Suppl 32–32):734–736. In: Proceedings of the 7th international conference on X-ray absorption fine structure, Kobe, Japan, 1992

Finger LW, Hazen RM (1980) Crystal structure and isothermal compression of Fe_2O_3, Cr_2O_3, V_2O_3 to 50 kbars. J Appl Phys 51(10):5362–5367

Frenkel A, Stern E, Voronel A, Heald S (1996) Lattice strain in disordered mixed salts. Solid State Commun 99(2):67–71

Gaudry E, Kiratisin A, Sainctavit Ph, Brouder Ch, Mauri F, Ramos A, Rogalev A, Goulon J (2003) Structural and electronic relaxations around substitutional Cr^{3+} and Fe^{3+} ions in corundum. Phys Rev B 67(9):094108

Graham J (1960) Lattice spacings and colour in the system alumina–chromic oxide. J Phys Chem Solids 17:18

Hahn T (ed) (1995) International tables for crystallography, vol A. The International Union of Crystallography

Hutter J, Ballone P, Bernasconi M, Focher P, Fois E, Goedecker S, Parrinello M, Tuckerman M (1996) CPMD version 3.0 mpi für Festkörperforschung. Stuttgart and IBM research

Kizler P, He J, Clarke DR, Kenway PR (1996) Structural relaxation around substitutional Cr^{3+}. J Am Ceram Soc 79(1):3–11

Langer K (2001) A note on mean distances, $R_{[MO_6]}$, in substituted polyhedra, $[(M_{1-x}M'_x)o_6]$, in the crystal structures of oxygen based solid solutions: local versus crystal averaging methods. Z Kristallogr 216:87–91

Lee Y, Reeder R, Wenskus R, Elzinga E (2002) Structural relaxation in the $MnCO_3$–$CaCO_3$ solid solution: a Mn K-edge EXAFS study. Phys Chem Miner 29:585–594

Levelut C, Ramos A, Petiau J, Robino M (1991) EXAFS study of the local structure in $CdSe_xSe_{1-x}$ compounds. Materials science and engineering, pp 251–263
Lever ABP (1984) Inorganic electronic spectroscopy. Elsevier, Amsterdam
Liehr AD (1963) The three electron (or hole) cubic ligand field spectrum. J Phys Chem 67:1314
MacFarlane RM (1963) Analysis of the spectrum of d^3 ions in trigonal crystal fields. J Chem Phys 39:3118
Marfunin AS (1979) Physics of minerals and inorganic materials. Springer, Berlin Heidelberg New York
Martins JL, Zunger A (1984) Bond lengths around isovalent impurities and in semiconductor solid solutions. Phys Rev B 30:6217–6220
McCauley JW, Gibbs GV (1972) Redetermination of the chromium position in ruby. Zeitschr f Kristallographie 135:453–455
McClure DS (1962) Optical spectra of transition metal ions in corundum. J Chem Phys 36:2757–2779
McClure DS (1963) Comparison of the crystal fields and optical spectra of Cr_2O_3 and ruby. J Chem Phys 38(9):2289
Moss SC, Newnham RE (1964) The chromium position in ruby. Zeitschr f Kristallographie 120:359–363
Nassau K (1983) The physics and chemistry of color. Wiley Interscience, New York
Pauling L (1967) The nature of the chemical bond. Cornell University Press, Ithaca
Pearson WB (1962) Structure reports, vol 27. International Union of Crystallography
Poole CP (1964) The optical spectra and color of chromium containing solids. J Phys Chem Solids 25:1169
Poole CP, Itzel JF (1963) Optical reflection spectra of chromia–alumina. J Chem Phys 39(12):3445
Reeder RJ, Lamble GM, Northrup P (1999) XAFS study of the coordination and local relaxation around Co^{2+}, Zn^{2+}, Pb^{2+}, and Ba^{2+} trace elements in calcite. Am Miner 84:1049–1060
Reinen D (1969) Ligand-field spectroscopy and chemical bonding in Cr^{3+}-containing oxidic solids. Struct Bond 6:30
Shannon RD (1976) Revised effective ionic radii and systematic studies of interatomic distances in halides and chalcogenides. Acta Crystallogr A32:751–767
Sugano S, Peter M (1961) Effect of configuration mixing and covalency on the energy spectrum of ruby. Phys Rev 122(2):381
Sugano S, Tanabe Y (1958) Absorption spectra of Cr^{3+} in Al_2O_3. J Phys Soc Jpn 13:880
Teo BK (1985) EXAFS: basic principles and data analysis. Springer, Berlin Heidelberg New York
Theil C, van Elp J, Folkman F (1999) Ligand field parameters obtained from and chemical shifts observed at the Cr $L_{2,3}$ edges. Phys Rev B 59(12):7931
Thole T, van der Laan G, Fuggle JC, Sawatzky G, Karnatak RC, Estava J-M (1985) 3*d* X-ray absorption lines and the $3d^9 4f^{n+1}$ multiplets of the lanthanides. Phys Rev B 32(8):5107–5118
Waychunas GA, Dollase WA, Ross CR (1994) Short-range order measurements in MgO–FeO and MgO–$LiFeO_2$ solid solutions by DLS simulation-assisted EXAFS analysis. Am Miner 79:274–288
Winterer M (1997) A data analysis program for material science. J Physique IV (Paris) 7(2):243
Wyckoff RWG (1964) Crystal structures, 2nd edn, vol 2. Wiley, New York